KSME

Springer

Journal of Mechanical Science and Technology 34 (8) 2020

Original Article
DOI 10.1007/s12206-020-0712-4

Keywords:
· Constant life diagram
· Longitudinal fatigue
· Mean stress effect
· S-N curve
· Unidirectional composites

Correspondence to:
Yuanchen Huang
yuanchen.huang@hotmail.com

Citation:
Huang, Y., Ha, S. K. (2020). A new constant life diagram model for the longitudinal fatigue of unidirectional composites. Journal of Mechanical Science and Technology 34 (8) (2020) 3207~3216.
http://doi.org/10.1007/s12206-020-0712-4

Received November 20th, 2019
Revised May 25th, 2020
Accepted June 1st, 2020

† Recommended by Editor Chongdu Cho

A new constant life diagram model for the longitudinal fatigue of unidirectional composites

Yuanchen Huang[1] and Sung Kyu Ha[2]

[1]Department of Mechanical Engineering, University of Shanghai for Science and Technology, 516 Jungong Road, Shanghai 200093, China, [2]Department of Mechanical Engineering, Hanyang University, 222 Wangsimni-ro, Seongdong-gu, Seoul 04763, Korea

Abstract A new constant life diagram (CLD) model featuring asymmetric bilinear constant-life curves was proposed to better describe the longitudinal fatigue behavior of unidirectional laminae (UD) under a wide range of stress ratios. This model is able to predict S-N curves with satisfactory accuracy not only in tension-tension (T-T) fatigue mode but also in tension-compression (T-C) and compression-compression (C-C) modes, whereas the conventional Goodman CLD model shows inferior performance especially in T-C and C-C modes. Apart from static tension and compression tests, high- and low-cycle fatigue tests at two stress ratios corresponding to T-T and C-C modes should be performed to determine the parameters in the proposed model. Fatigue test data of several different GFRP UDs at various stress ratios were utilized to validate the proposed model, and the S-N curves predicted by the proposed model agreed well with the experimental results. Compared with the Goodman CLD model, the proposed CLD model demonstrates an enhanced predictive capability without losing its simplicity.

1. Introduction

With the increasingly extensive application of continuous fiber-reinforced composites in major load-bearing components in large structures such as the fuselage and wing box of intercontinental airliners, the blades of megawatt wind turbines, and the risers in deepwater oil platforms, the durability of these composites against fatigue loading has received much attention from both the industry and academia. Given that the longitudinal direction of unidirectional laminae (UD) is the main load-carrying direction, understanding longitudinal fatigue behavior is the most important step in establishing a fatigue life prediction methodology that is universally applicable to multi-directional laminates and other composites with various fiber architectures. Furthermore, the UD longitudinal response under tension-compression (T-C) and compression-compression (C-C) fatigue should be treated as important as that under tension-tension (T-T) fatigue because T-C and C-C loadings are no less common than T-T in reality. For instance, during the normal operation of a wind turbine blade, the spar cap on the pressure side is mainly subject to T-T fatigue, whereas that on the suction side is under C-C fatigue as illustrated in Fig. 1.

The constant life diagram (CLD) presents a straightforward yet comprehensive description of the correlation among mean stress σ_{mean}, stress amplitude σ_{amp}, and number of cycles to failure N_{f} under uniaxial constant amplitude loading. Introduced in the late 19th century [1], the CLD is widely used in assessing the fatigue life of not only metals but also that of composites despite its phenomenological nature. Currently, the Goodman CLD model and its variants are the most popular types of CLDs that have been accepted by major certification agencies, such as Germanischer Lloyd and Det Norske Veritas, as the main approach for evaluating the fatigue life of fiber-reinforced plastics (FRP) in wind turbines [2, 3]. Nevertheless, the poor accuracy of the Goodman CLD model for composites has been widely debated by researchers. Harris et al. [4-7] proposed bell-shaped constant-life curves determined by a formula with three parameters that are functions of N_{f}.

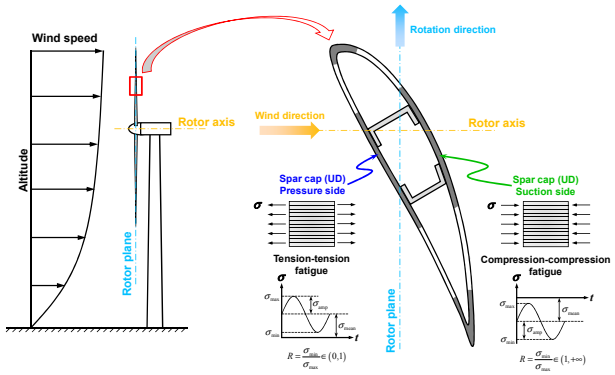

Fig. 1. Schematic illustration of fatigue loadings applied to spar caps in a wind turbine blade during its operation: T-T on the pressure side, and C-C on the suction side.

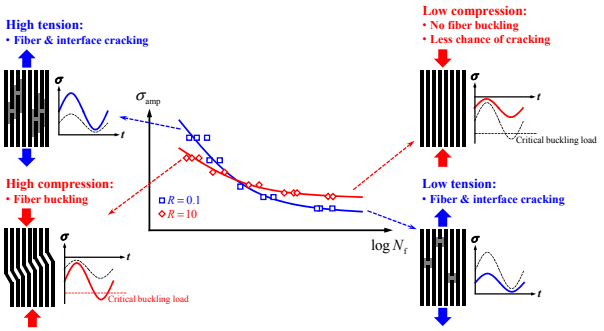

Fig. 2. Typical S-N curves of GFRP UD under T-T and C-C fatigue loadings.

Kawai and Koizumi [8] developed an anisomorphic CLD model for composite laminates that can be constructed by using laminate static tensile strength T (> 0) and compressive strength C (> 0) together with the S-N curve obtained at the critical stress ratio $\chi \equiv -C/T$. Each constant-life curve comprises two smooth segments that are connected at the point corresponding to χ . Kawai and Murata [9] later modified this formulation by inserting a transitional segment in the constant-life curve between χ and the newly defined sub-critical stress ratio χ_S to improve the prediction accuracy for angle-ply ($[\pm30]_{3S}$, $[\pm45]_{3S}$, $[\pm60]_{3S}$) carbon/epoxy laminates. Kawai et al. [10, 11] also introduced temperature dependence in the CLD formulation and demonstrated its effectiveness in predicting the fatigue life of woven carbon fabric/epoxy laminates at multiple temperature levels. The anisomorphic CLD model is constantly evolving to enable its application to carbon/epoxy UD under off-axis fatigue loading [12], woven carbon/epoxy laminates under fatigue loading with alternating stress ratios [13], carbon/epoxy UD while considering failure probability [14], and woven carbon/epoxy laminates under fatigue loading with alternating stress ratios and non-proportional loading paths [15]. Broer and Zarouchas [16] developed their own version of the anisomorphic CLD model that comprises two sub-models, one of which is applicable to laminates whose ultimate tensile strength is greater than the ultimate compressive strength, whereas the other is applicable to laminates with inverse characteristics. Instead of fitting fatigue test data, Kassapoglou [17, 18] derived and validated a CLD formulation based on the assumption of a constant cycle-by-cycle failure probability under constant amplitude loading. Vassilopoulos et al. compared the predictive capability of several existing CLD formulations [18] and proposed a piecewise non-linear CLD model by interpreting fatigue data plotted on an $R-\sigma_{amp}$ plane [20]. Given the lack of satisfactory models, numerous time-consuming fatigue tests need to be conducted to acquire sufficient data for constructing CLDs for a variety of multi-directional laminates [21, 22].

Rather than being overwhelmed by the complexity of CLDs for multi-directional laminates, we revisited the UD longitudinal test data under T-T and C-C constant amplitude loadings. A common observation was that the S-N curves fitted by using C-C fatigue test data appear flatter than those fitted by using T-T test data. Particularly for GFRP UDs, the T-T and C-C S-N curves (typically with stress ratios of R = 0.1 and 10) usually intersect with each other when plotted on an $\sigma_{amp}-\log N_f$ plane, where σ_{amp} represents the stress amplitude. Such phenomenon have been rarely described in the literature and in any of the aforementioned models, including the Goodman CLD model. The differences among the S-N curves reflect an intrinsic UD longitudinal response to T-T and C-C fatigue loadings that cannot be overlooked. Therefore, we propose a new CLD model with an aim to provide a highly accurate description of the overall UD longitudinal fatigue behavior, particularly under T-C and C-C modes.

2. New CLD model

2.1 Model development

Fig. 2 shows typical T-T and C-C S-N curves for GFRP UDs. Such behavior is quite understandable; materials tend to show stronger resistance against fatigue loading in the C-C mode than in the T-T mode because the propagation of cracks is suppressed in the former yet is promoted in the latter. However, fibers in a UD buckle easily under a high C-C fatigue load in the longitudinal direction, thereby leading to structural failure in the micro-scale prior to material failure.

By contrast, a typical Goodman CLD for UD longitudinal fatigue [2] has isosceles triangular constant-life curves that are anchored to the horizontal axis at X and $-X'$ as shown on the left side of Fig. 3. The Goodman CLD model requires one experimentally obtained S-N curve (usually in T-T mode) to determine the evolution of constant-life curves versus N_f ; nevertheless, as explained in the preceding paragraphs, different failure mechanisms are involved in T-T and C-C fatigue. In this case, the information carried by one S-N curve cannot sufficiently characterize UD fatigue behavior in a wide range of stress ratios. Naturally, the T-T and C-C S-N curves generated from the Goodman CLD model are unable to describe the crossing-over phenomenon as illustrated on the right side of Fig. 3.

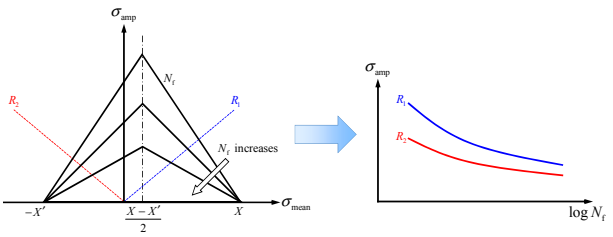

Fig. 3. Typical Goodman CLD for UD longitudinal fatigue and the resulting T-T and C-C S-N curves.

The target of the new CLD model is to accurately describe UD longitudinal fatigue behavior under T-T, T-C, and C-C modes while retaining the simplicity of the Goodman model. Accordingly, the new CLD model has the following features:

1) The constant-life curves in the proposed CLD are still bilinear, with UD longitudinal tensile strength X (>0) and compressive strength $-X'$ (<0) serving as two anchor points on the horizontal axis similar to the Goodman model.

2) Bilinear constant-life curves can be asymmetric and gradually bias leftward as N_f increases, thereby resulting in a relatively sparse distribution of the right-side segments of constant-life curves and the relatively dense distribution of their left-side counterparts.

3) Two experimentally determined S-N curves, one of which is in the T-T mode and the other is in the C-C mode, are required to define the dependency of the shape of constant-life curves on N_f.

2.2 Formulation of the new CLD model

Based on the aforementioned features, the newly proposed CLD model (hereinafter referred to as the HH model) for UD longitudinal fatigue is formulated as

$$\begin{cases} \sigma_{eff} = \dfrac{\sigma_{amp} T}{\beta\sigma_{mean} + \dfrac{(T+C)-\beta(T-C)}{2} - \left|\sigma_{mean} - \dfrac{(T-C)-\beta(T+C)}{2}\right|} \\ \sigma_{eff} = bN_f^{\frac{1}{n}} \end{cases} \tag{1}$$

where σ_{eff} is the stress-ratio-independent effective stress corresponding to the given number of cycles to failure N_f, β controls the deviation of the peak of the constant-life curve from the centerline between X and $-X'$, and β is assumed as a linear function of N_f in log-scale:

$$\beta = \frac{1}{\mu}\log N_f + \beta_0 . \tag{2}$$

Parameters b, n, μ, and β_0 are constants that are to be determined from the experimentally obtained T-T and C-C S-N curves.

The geometric characteristics of the new CLD model are illustrated in Fig. 4. The peak of the constant-life curve deviates horizontally by $|\beta|(X+X')/2$ from the centerline between two anchor points and serves as the axis of symmetry in the Goodman CLD model. When $\sigma_{mean} = \left[(X-X')-\beta(X+X')\right]/2$ is substituted into Eq. (1), the vertical coordinate of the peak is calculated as

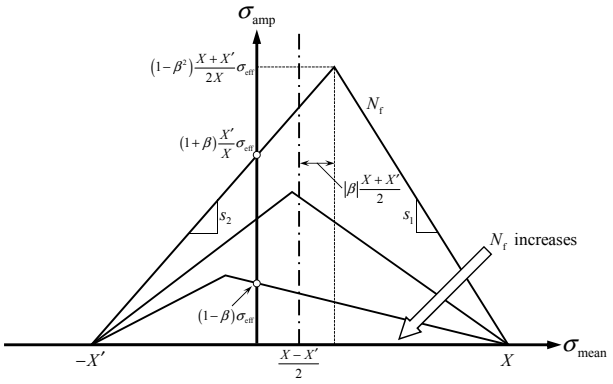

Fig. 4. Geometric characteristics of HH CLD.

$$\sigma_{amp} = (1-\beta^2)\frac{X+X'}{2X}\sigma_{eff} . \tag{3}$$

Depending on the sign of the horizontal coordinate of the peak, the intercept of the constant-life curve on the vertical axis can be calculated by substituting $\sigma_{mean} = 0$ into Eq. (1):

$$\sigma_{amp} = \begin{cases} (1+\beta)\dfrac{X'}{X}\sigma_{eff} & \sigma_{mean} \geq \dfrac{(X-X')-\beta(X+X')}{2} \\ (1-\beta)\sigma_{eff} & \sigma_{mean} < \dfrac{(X-X')-\beta(X+X')}{2} \end{cases} . \tag{4}$$

If the slopes of the right- and left-side segments of the bilinear constant-life curve are denoted by s_1 and s_2, respectively, then the horizontal coordinate of the peak can be re-expressed in terms of those slopes as

$$\sigma_{mean} = \frac{s_1 X + s_2 X'}{s_1 - s_2} . \tag{5}$$

When the right-side of Eq. (5) is equated to $\left[(X-X')-\beta(X+X')\right]/2$, which is the horizontal coordinate of the peak, β can be related to those slopes as

$$\beta = \frac{s_2 + s_1}{s_2 - s_1} . \tag{6}$$

Similarly, the vertical coordinate of the peak can be expressed in terms of s_1 and s_2 as

$$\sigma_{amp} = \frac{s_1 s_2}{s_1 - s_2}(X + X') . \tag{7}$$

By equating the right-sides of Eqs. (3) and (7) and by using Eq. (6), σ_{eff} can be related to these slopes as

$$\sigma_{\text{eff}} = \frac{s_2 - s_1}{2} X . \tag{8}$$

Eqs. (6) and (8) are especially useful in determining parameters b, n, m, and β_0.

2.3 Procedures of parameter determination

Parameters b, n, μ, and β_0 in Eqs. (1) and (2) can be determined as follows:

(a) Perform UD longitudinal fatigue tests at a minimum of two load levels, one in the low-cycle region and the other in the high-cycle region, in both T-T and C-C modes. T-T fatigue tests should be conducted following ASTM D3479/D3479M-19 or its equivalent standards, whereas C-C fatigue tests should be carried out by referring to ASTM D3410/D3410M-16 and its related standards. At least three test data should be generated at each load level to ensure statistical consistency. Load levels and stress ratios should be adjusted according to need.

(b) Fit the test data by using Eq. (9) to obtain analytical expressions of the T-T and C-C S-N curves.

$$\sigma_{\text{amp}} = cN_{\text{f}}^{-\frac{1}{m}} \tag{9}$$

(c) Select one fatigue life in the low-cycle region (denoted by $N_{\text{f},1}$) and one in the high-cycle region (denoted by $N_{\text{f},2}$). Denote the points corresponding to $N_{\text{f},1}$ on the T-T and C-C S-N curves by points 1 and 2 and those corresponding to $N_{\text{f},2}$ by points 3 and 4. Mark points 1, 2, 3, and 4 on the $\sigma_{\text{mean}} - \sigma_{\text{amp}}$ plane.

(d) Connect the anchor point X located on the positive horizontal axis and point 1 as well as the other anchor point $-X'$ located on the negative horizontal axis and point 2 by using straight lines. Extend these two lines until they intersect, and a bilinear constant-life curve corresponding to $N_{\text{f},1}$ is constructed.

(e) Denote the slopes of line segments passing through points 1 and 2 by s_1 and s_2, respectively. The slope of each segment can be calculated as

$$\begin{cases} s_1 = \dfrac{\sigma_{\text{amp}}^{(1)}}{\sigma_{\text{mean}}^{(1)} - X} & R \in (0,1) \\ s_2 = \dfrac{\sigma_{\text{amp}}^{(2)}}{\sigma_{\text{mean}}^{(2)} + X'} & R \in (1,+\infty) \end{cases} \tag{10}$$

where $\sigma_{\text{mean}}^{(i)}$ and $\sigma_{\text{amp}}^{(i)}$ are the coordinates of point i.

(f) Calculate β_1 and $\sigma_{\text{eff},1}$ corresponding to $N_{\text{f},1}$ by using Eqs. (6) and (8), respectively.

(g) Repeat steps (d) to (f) to construct a constant-life curve corresponding to $N_{\text{f},2}$, and calculate β_2, $\sigma_{\text{eff},2}$ accordingly.

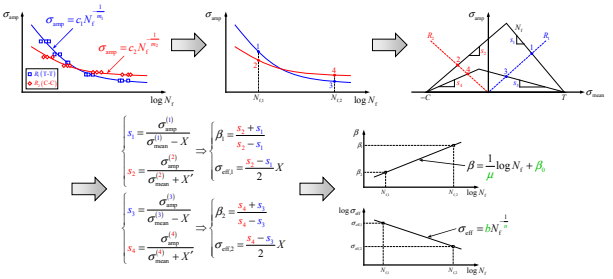

Fig. 5. Schematic explanation of the procedures for determining the parameters in the HH CLD model.

(h) Determine b, n by using $\sigma_{\text{eff},1}$, $\sigma_{\text{eff},2}$, and Eq. (1), and determine μ, β_0 by using β_1, β_2, and Eq. (2).

All of the above procedures are shown schematically in. When parameters b, n, μ, and β_0 are determined, the constant-life curves corresponding to any N_{f} can be easily generated. As a result, the S-N curve for any stress ratio can be determined graphically. First, draw a radial line from the origin of the $\sigma_{\text{mean}} - \sigma_{\text{amp}}$ plane to represent the stress ratio in need. Second, replot all intersecting points between the radial line and constant-life curves on the conventional $\sigma_{\text{amp}} - \log N_{\text{f}}$ plane. Third, connect these points on the $\sigma_{\text{amp}} - \log N_{\text{f}}$ plane by using a smooth curve, and the construction of one S-N curve is completed.

3. Model verification

To verify the HH CLD model, UD longitudinal fatigue test data at multiple stress ratios are needed, particularly those under the T-T and C-C modes, which are important in model parameter determination. However, not many data are available for UD longitudinal C-C fatigue partially due to the difficulties in preventing premature failure modes, such as buckling during tests. A limited amount of UD test data that meet our requirement can be found in Ref. [23]. Two GFRP UDs, denoted by UNI-D155B-UP2 and UNI-D072A-UP2 in the reference, were used to highlight the difference between CLDs and the predicted S-N curves based on the HH and Goodman models. The fiber used in UNI-D155B-UP2 and UNI-D072A-UP2 are Knytex D155 (E-glass, 527 gsm) and Knytex D072 (E-glass, 230 gsm), respectively, whereas the matrix used in the two UDs is CoRezyn 63-AX-051 polyester with 1 % MEKP. The volume fractions of these fibers are 0.4 and 0.33, respectively. Table 1 summarizes the material information of UNI-D155B-UP2 and UNI-D072A-UP2.

As previously described, the first step in determining the parameters of the HH model is curve fitting for T-T and C-C fatigue test data. For both materials, the T-T S-N curve was fitted by using test data at R = 0.1, and the C-C S-N curves were fitted by using test data at R = 10. For UNI-D155B-UP2, the fitted values of parameters c, m in Eq. (9) are 467.09 MPa and 12.35 for R = 0.1 and 300.62 MPa and 21.93 for R = 10. For UNI-D072A-UP2, the fitted values of c, m in Eq. (9) are

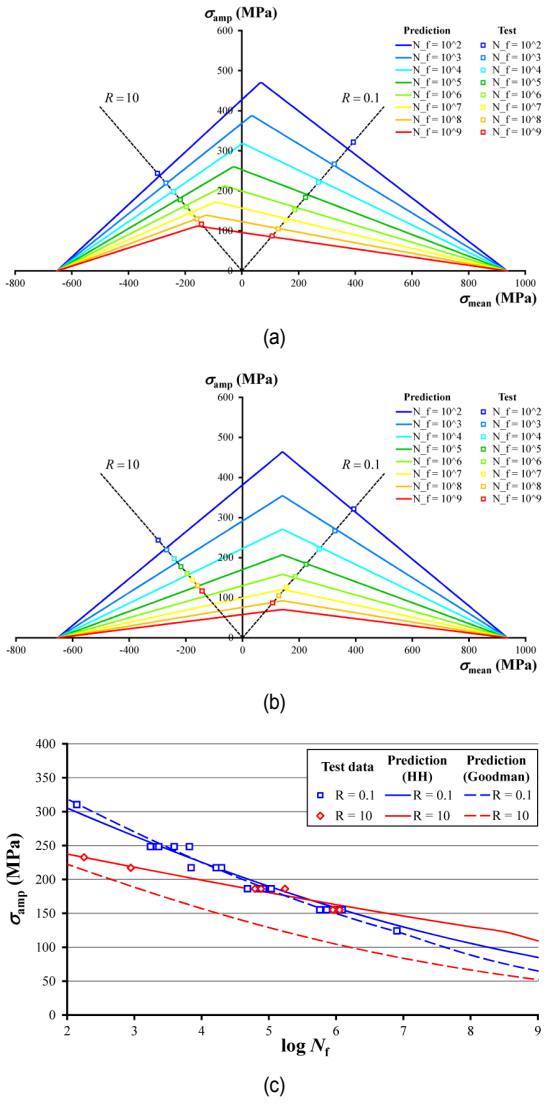

Fig. 6. Comparison of the test data with the (a) CLD based on the HH model; (b) CLD based on the Goodman model; (c) S-N curves predicted by both the HH and Goodman models for UNI-D155B-UP2.

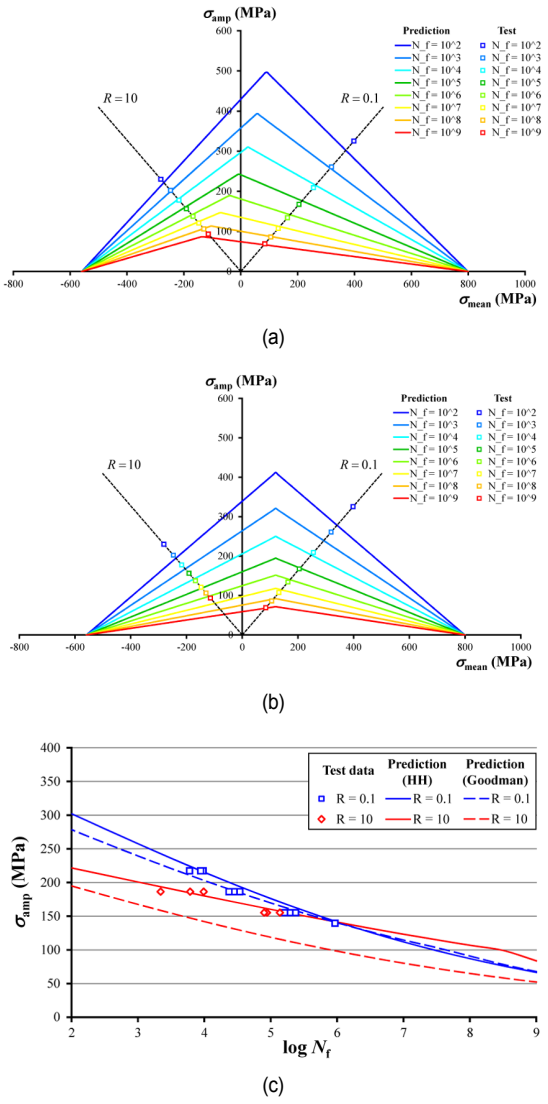

Fig. 7. Comparison of the test data with the (a) CLD based on the HH model; (b) CLD based on the Goodman model; (c) S-N curves predicted by both the HH and Goodman models for UNI-D072A-UP2.

506.66 MPa and 10.41 for R = 0.1 and 297.46 MPa and 17.91 for R = 10. As mentioned in step (c) of Sec. 2.3, after obtaining the expressions of the T-T and C-C S-N curves, two N_f values should be selected to compute the model parameters. For both materials, $N_{f,1}$ and $N_{f,2}$ were set to 10^3 and 10^8 cycles, respectively. The following model parameters were then determined: $b = 810.90$ MPa, $n = 12.46$, $\mu = 24.81$, and $\beta_0 = 0.0134$ for UNI-D155B-UP2, and $b = 926.43$ MPa, $n = 10.11$, $\mu = 21.00$, and $\beta_0 = -0.0511$ for UNI-D072A-UP2. For comparison, constant-life curves based on both the HH and Goodman models in the GL guideline [2] were constructed for both materials. The only parameter in the Goodman model (the slope parameter m) was determined by using the T-T test data for each material. The values of m were 8.56 and 9.22 for UNI-D155B-UP2 and UNI-D072A-UP2, respectively. The parameters for both the Goodman and HH models are listed in Tables 1 and 2, respectively.

Figs. 6(a) and (b) show the CLDs based on the HH and Goodman models, respectively, for UNI-D155B-UP2. In both figures, 8 constant-life curves corresponding to N_f ranging from 10^2 to 10^9 cycles were plotted with the test data. Colors were used to differentiate the constant-life curves and test data corresponding to different N_f. The slope parameter m in the Goodman model for UNI-D155B-UP2 was 8.56, whereas the reference value in the GL guideline was 9 for UD with the polyester matrix [2]. Fig. 6(a) shows an excellent agreement between the HH CLD and test data in the entire range of N_f, while the Goodman CLD data well match the T-T test data (R = 0.1) yet underestimate the C-C test data (R = 10). The difference between the Goodman prediction and test data increases along with N_f as shown in Fig. 6(b). Fig. 6(c) compares the test data with the S-N curves for R = 0.1 and 10 as predicted

by both the HH and Goodman models and offers another perspective toward the predictive capability of both models. Both the T-T and C-C test data are well described by the S-N curves based on the HH model, whereas the Goodman model only captures the T-T test data yet deviates far from the C-C test data. Such observation agrees with Figs. 6(a) and (b). The T-T and C-C S-N curves predicted by the HH model intersect with each other, whereas their counterparts predicted by the Goodman model tend to approach each other but never intersect.

Figs. 7(a) and (b) show the CLDs based on the HH and Goodman models, respectively, for UNI-D072A-UP2. In this case, the slope parameter m in the Goodman model was 9.22, while the reference value is 9 in the GL guideline [2]. Similar to the previous case, an excellent agreement was observed between the test data and the constant-life curves based on the HH model, while the Goodman model only offers a satisfactory description of the T-T test data yet underestimates the C-C test data.

The above finding is understandable. Given that both the T-T and C-C S-N curves were employed to determine the parameters in the HH model, the HH CLD can reflect both T-T and C-C behavior. However, only the T-T test data were used to determine the parameters in the Goodman model. Therefore, the Goodman CLD lacks sufficient information regarding C-C behavior. The T-T and C-C S-N curves predicted by the HH model pass through their corresponding test data accurately. The T-T S-N curve predicted by the Goodman model is close to its counterpart predicted by the HH model, whereas the C-C S-N curve predicted by the Goodman model is far from the test data as shown in Fig. 7(c).

As shown in the previous two cases, the advantage of the HH model over the conventional Goodman model lies in its description of the C-C fatigue behavior of UD. Nevertheless, the accuracy of the HH model in describing UD fatigue behavior under other loading modes, such as T-C, needs to be estimated. Therefore, two additional UD materials were used, namely, glass/epoxy from our industrial partner (denoted by UD-1) and the glass/polyester in Ref. [23] (denoted by UNI-(0)2-UP2). The matrix used in UD-1 was the epoxy resin system constituted by EPIKOTE™ Resin MGS® RIMR135 and EPIKURE™ Curing Agent MGS® RIMR 137 from Momentive Special Chemicals Inc. mixed in a ratio of 100:30 by weight. However, the fiber was proprietary, and the product name was undisclosed. UD-1 has a fiber volume fraction of 0.56, whereas the other material, UNI-(0)2-UP2, has the same constituents as UNI-D155B-UP2 but with a higher fiber volume fraction ($V_f = 0.5$). Table 1 summarizes the material information of UD-1 and UNI-(0)2-UP2. The longitudinal fatigue test data for both materials were available at R = 0.1, 10, and -1, and the T-T (R = 0.1) and C-C (R = 10) data were fitted by using Eq. (9). For UD-1, the fitted parameters c, m in Eq. (9) are 583.90 MPa and 11.90 for R = 1 and 443.84 MPa and 27.38 for R = 10. For UNI-(0)2-UP2, the fitted parameters are 635.82 MPa and 11.05 for R = 0.1 and 274.99 MPa and 20.72 for R = 10. For both materials, $N_{f,1}$ and $N_{f,2}$ were set to 10^3 and 10^8 cycles, which yield the following parameters in the HH model: $b = 1060.47$ MPa, $n = 13.31$, $\mu = 19.26$, and $\beta_0 = 0.0337$ for UD-1, and $b = 1083.32$ MPa, $n = 12.23$, $\mu = 24.39$, and $\beta_0 = 0.1107$ for UNI-(0)2-UP2. By contrast, the slope parameter m in the Goodman model was determined from the T-T fatigue test data as 9.06 and 9.18 for UD-1 and UNI-(0)2-UP2, respectively. The parameters for both the Goodman and HH models are listed in Tables 1 and 2.

Table 1. Material information of all types of UDs employed in this study.

	UNI-D155B-UP2 [23]	UNI-D072A-UP2 [23]	UD-1	UNI-(0)2-UP2 [23]
Fiber	Knytex D155 (E-glass, 527 gsm)	Knytex D072 (E-glass, 230 gsm)	E-glass (product name classified)	Knytex D155 (E-glass, 527 gsm)
Matrix	CoRezyn 63-AX-051 polyester with 1 % MEKP	CoRezyn 63-AX-051 polyester with 1 % MEKP	EPIKOTE™ Resin MGS® RIMR135 and EPIKURE™ Curing Agent MGS® RIMR 137	CoRezyn 63-AX-051 polyester with 1 % MEKP
V_f	0.4	0.33	0.56	0.5
E (GPa)	32.7	28.5	-	39.2
X (MPa)	936	799	1066	1430
X' (MPa)	653	559	907	608

Table 2. Parameters in the Goodman model for all types of UDs employed in this study.

	UNI-D155B-UP2	UNI-D072A-UP2	UD-1	UNI-(0)2-UP2
m	8.56	9.22	9.06	9.18

Table 3. Parameters in the HH model for all types of UDs employed in this study.

	UNI-D155B-UP2	UNI-D072A-UP2	UD-1	UNI-(0)2-UP2
b (MPa)	816.90	926.43	1060.47	1083.32
n	12.46	10.11	13.31	12.23
μ	24.81	21.00	19.26	24.39
β_0	0.0134	-0.0511	0.0337	0.1107

The CLDs for UD-1 based on the HH and Goodman models are presented in Figs. 8(a) and (b). The stresses corresponding to different N_f values for R = 0.1, 10, and -1 were back-calculated from the S-N curves that were fitted by using fatigue test data and were superposed onto all CLDs to provide a straightforward assessment of accuracy. Fig. 8(a) shows that the test data at R = 0.1 and 10 are close to their corresponding constant-life curves, except that for R = 10, the stresses in the high-cycle region ($N_f \geq 10^7$) predicted by the CLD are lower than the test data. The test data of R = -1 (i.e., along the vertical axis) are satisfactorily described by HH CLD except for a

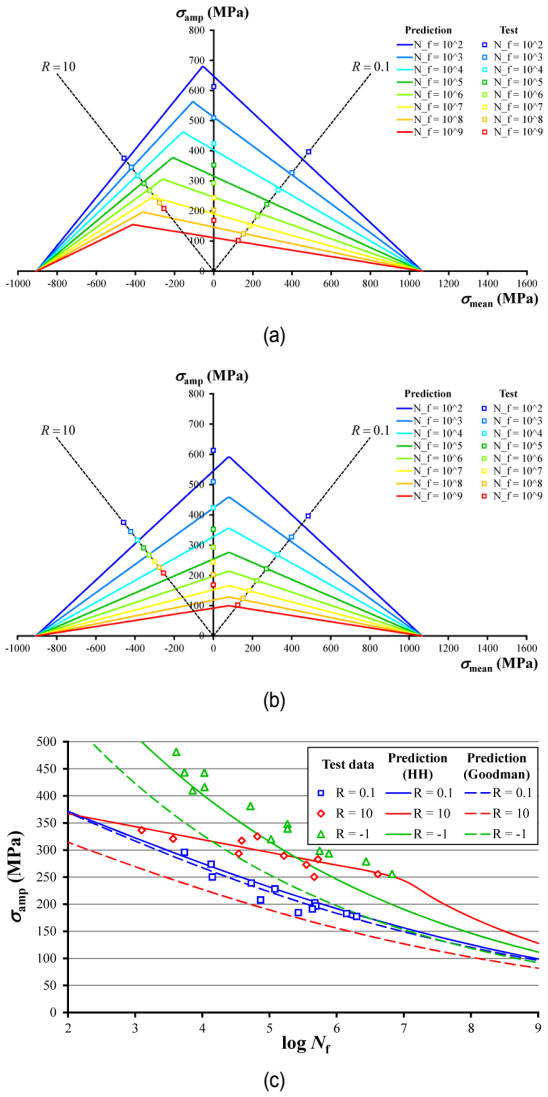

Fig. 8. Comparison of the test data with (a) CLD based on the HH model; (b) CLD based on the Goodman model; (c) S-N curves predicted by both the HH and Goodman models for UD-1.

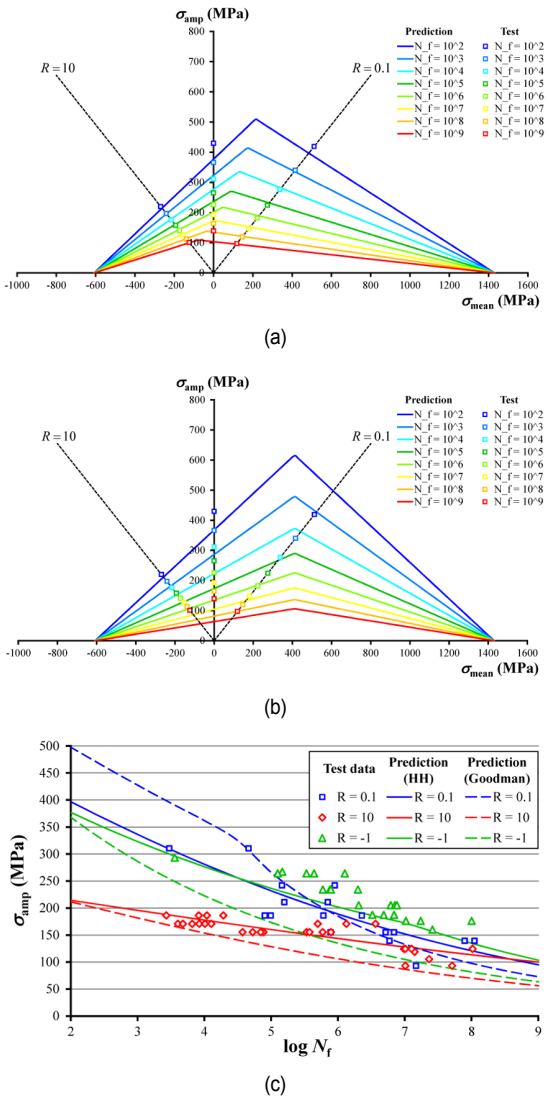

Fig. 9. Comparison of the test data with the (a) CLD based on the HH model; (b) CLD based on the Goodman model; (c) S-N curves predicted by both the HH and Goodman models for UNI-(0)2-UP2.

minor underestimation in the high-cycle region. However, the Goodman CLD greatly underestimates the T-C test data at R = -1, and the situation worsens when compared with the test data at R = 10 as shown in Fig. 8(b). Although the Goodman CLD still matches the T-T test data at a relatively high accuracy, its overall performance is inferior to that of the HH model. Fig. 8(c) compares the test data of R = 0.1, 10, and -1 with the S-N curve for the stress ratios predicted by both the HH and Goodman models. The S-N curves predicted by the HH model passes through most of their corresponding data points, only the S-N curve for R = 0.1 predicted by the Goodman model agrees well with the test data, and the S-N curves for the other two stress ratios predicted by the Goodman model deviate far from the test data.

One noteworthy phenomenon is the sudden turning of the S-N curve for R = 10 predicted by the HH model, which appears near $N_f = 10^7$ cycles. The HH CLD in Fig. 8(a) shows that the dashed radial line, which represents R = 10, intersects with the left-half segments of constant-life curves when $N_f \le 10^7$. Meanwhile, when $N_f > 10^7$, the radial line intersects with the right-half segments.

Such transition occurs when N_f is between 10^7 and 10^8, which directly leads to a large difference between the intersections of the radial line and the two constant-life curves for $N_f = 10^7$ and $N_f = 10^8$. Such phenomenon can only be avoided if the peaks of all bilinear constant-life curves fall along a straight line passing through the origin.

Figs. 9(a) and (b) show the CLDs based on the HH and Goodman models for UNI-(0)2-UP2 together with the test data at R = 0.1, 10, and -1. The HH CLD well predicts both T-T and C-C test data yet slightly underestimates the T-C test data. Meanwhile, the Goodman CLD overestimates the test data at

R = 0.1 in the low-cycle region and underestimates the test data in the high-cycle region; for *R* = 10 and -1, the test data are mostly underestimated by the Goodman CLD. Fig. 9(c) clearly shows that the test data at *R* = 0.1 and 10 are well described by the S-N curves predicted by the HH model for the corresponding stress ratios, whereas the S-N curve for *R* = 0.1 predicted by the Goodman model well matches the test data. However, the agreement for *R* = 10 is poor. A turning point appears near $\log N_f = 4.5$ on the S-N curve of *R* = 0.1 predicted by the Goodman model primarily due to the vertically aligned peaks of the constant-life curves from the Goodman model. For *R* = -1, the S-N curve from the HH model outperforms its counterpart from the Goodman model. The comparison between the predictive capability of the HH and Goodman models reveals that due to insufficient information, the accuracy of the Goodman model in a wide range of stress ratios cannot be guaranteed, while the performance of the HH CLD model is quite stable and insensitive to material type.

4. Discussion and conclusion

The HH model for UD longitudinal fatigue was introduced in this work. This model aims to offer a better prediction of UD longitudinal behavior under T-T, T-C, and C-C fatigue modes. Therefore, two S-N curves at T-T and C-C fatigue modes are required to define the parameters in the HH model, and each S-N curve should be fitted by using the fatigue test data obtained at a minimum of two load levels. A systematic procedure for CLD construction and parameter determination was then proposed.

Test data for two glass/polyester UDs were employed to construct CLDs based on both the HH and conventional Goodman models for comparison. The CLD based on the HH model can accurately describe the test data at *R* = 0.1 and 10, whereas the CLD based on the Goodman model can only predict the test data at *R* = 0.1 and is unable to describe the test data at *R* = 10. The S-N curves at *R* = 0.1 and 10 reproduced from the HH CLD agreed well with the test data, while the Goodman model has a much inferior predictive capability.

Another batch of UD longitudinal fatigue test data for glass/epoxy and glass/polyester at *R* = 0.1, 10, and -1 was utilized to further evaluate the performance of the HH CLD model. The HH model not only predicts the test data at *R* = 0.1 and 10 but also offers satisfactory predictions at *R* = -1.

The test data at *R* = -1 in the high-cycle region were often slightly underestimated by the HH model, thereby suggesting that further improvements must be introduced in the future to better describe UD longitudinal T-C fatigue.

The formulation of the HH CLD model (i.e. Eq. (1)) was compared with that of the Goodman model in the GL guideline as follows [2]:

$$N_f = \left[\frac{(X+X') - |2\sigma_{mean} - (X-X')|}{2\sigma_{amp}}\right]^m . \quad (11)$$

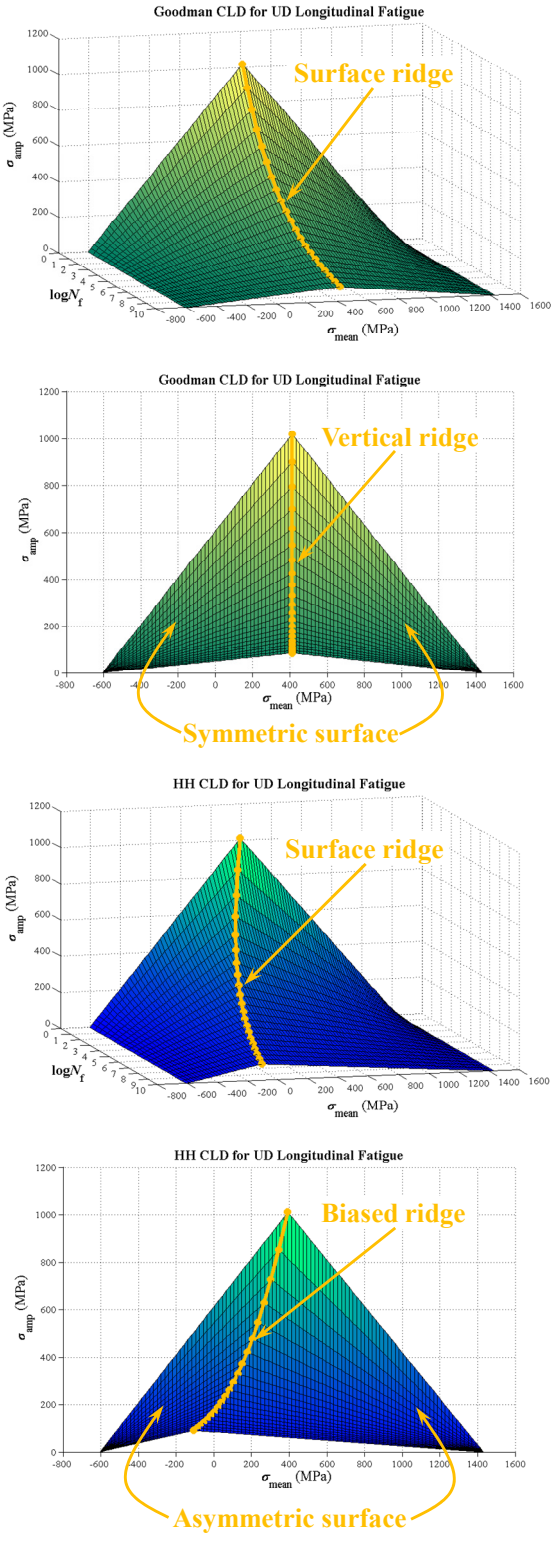

Fig. 10. Comparison between the 2D and 3D views of HH CLD and Goodman CLD.

When β in the HH model vanishes and when b is equal to X, the expression of the HH model reduces exactly to Eq. (11). Furthermore, the fatigue test data in the Goodman model

only determine one parameter, namely, the slope parameter m, while the HH model has four parameters, thereby suggesting that more information about fatigue behavior can be included in this model, hence improving its predictive capability. In this sense, the HH model is a generalization of the Goodman model. Both the HH and Goodman models describe a surface in a 3D space ($\sigma_{\text{mean}} - \sigma_{\text{amp}} - N_{\text{f}}$), and CLDs are simply projections of a 3D surface onto a $\sigma_{\text{mean}} - \sigma_{\text{amp}}$ plane as illustrated in Fig. 10. The Goodman CLD has two horizontally symmetric surfaces that are joined along a vertically moving curve (ridge), whereas the HH CLD bears the characteristics of two asymmetric surfaces with a ridge that horizontally biases toward the negative σ_{mean} side as N_{f} increases. Although the required number of fatigue tests has doubled for the HH model, considering the enhanced predictive capability in the T-C and C-C fatigue modes, these extra efforts are deemed worthwhile trade-offs.

In sum, the proposed HH CLD model is a simple yet effective tool for predicting the life of UD under longitudinal fatigue. Compared with the conventional Goodman model, the HH model requires few additional efforts for material characterization yet is able to describe UD longitudinal fatigue behavior under the T-T, T-C, and C-C loading modes with satisfactory accuracy. Although the HH model is initially proposed for UD longitudinal fatigue, its concept and procedures can be applied to any material that exhibits different fatigue behavior under T-T and C-C fatigue. This model has been proven effective yet is still phenomenological. Additional solid physical explanations will be provided in future work.

Nomenclature

σ_{mean}	: Mean stress
σ_{amp}	: Stress amplitude
R	: Stress ratio
N_{f}	: Number of cycles to failure
X	: Ply longitudinal tensile strength
X'	: Ply longitudinal compressive strength
σ_{eff}	: Stress-ratio-independent effective stress corresponding to the given number of cycles to failure
b, n, μ, β_0	: Shape parameters of the new constant life diagram
s_1, s_2	: Slopes of the right half and left half segments of the bilinear constant life curve

References

[1] G. P. Sendeckyj, Constant life diagrams - A historical review, *International Journal of Fatigue*, 23 (4) (2001) 347-353.

[2] *Guideline for the Certification of Wind Turbines*, Edition 2010, Germanischer Lloyd, Hamburg (2010).

[3] *Guidelines for Design of Wind Turbines*, Second edition, Det Norske Veritas, Copenhagen, and Wind Energy Department, Risø National Laboratory (2002).

[4] T. Adam, G. Fernando, R. F. Dickson, H. Reiter and B. Harris, Fatigue life prediction for hybrid composites, *International Journal of Fatigue*, 11 (4) (1989) 233-237.

[5] B. Harris, H. Reiter, T. Adam, R. F. Dickson and G. Fernando, Fatigue behavior of carbon fiber reinforced plastics, *Composites*, 21 (3) (1990) 232-242.

[6] N. Gathercole, H. Reiter, T. Adam and B. Harris, Life prediction for fatigue of T800/5245 carbon-fiber composites: I. Constant-amplitude loading, *International Journal of Fatigue*, 16 (8) (1994) 523-532.

[7] B. Harris, A parametric constant-life model for prediction of the fatigue lives of fiber-reinforced plastics, B. Harris (editor), *Fatigue in Composites*, Woodhead Publishing Limited (2003) 546-568.

[8] M. Kawai and M. Koizumi, Nonlinear constant fatigue life diagrams for carbon/epoxy laminates at room temperature, *Composites Part A*, 38 (11) (2007) 2342-2353.

[9] M. Kawai and T. Murata, A three-segment anisomorphic constant life diagram for the fatigue of symmetric angle-ply carbon/epoxy laminates at room temperature, *Composites Part A*, 41 (10) (2010) 1498-1510.

[10] M. Kawai and Y. Matsuda, Anisomorphic constant fatigue life diagrams for a woven fabric carbon/epoxy laminate at different temperatures, *Compos Part A*, 43 (4) (2012) 647-657.

[11] M. Kawai, Y. Matsuda and R. Yoshimura, A general method for predicting temperature-dependent anisomorphic constant fatigue life diagram for a woven fabric carbon/epoxy laminate, *Compos Part A*, 43 (6) (2012) 915-925.

[12] M. Kawai and N. Itoh, A failure-mode based anisomorphic constant life diagram for a unidirectional carbon/epoxy laminate under off-axis fatigue loading at room temperature, *Journal of Composite Materials*, 48 (5) (2014) 571-592.

[13] M. Kawai, K. Yang and S. Oh, Effect of alternating R-ratios loading on fatigue life of woven fabric carbon/epoxy laminates, *Journal of Composite Materials*, 49 (27) (2015) 3387-3405.

[14] M. Kawai and K. Yano, Anisomorphic constant fatigue life diagrams of constant probability of failure and prediction of P-S-N curves for unidirectional carbon/epoxy laminates, *International Journal of Fatigue*, 83 (2) (2016) 323-334.

[15] M. Kawai and Y. Ishizuka, Fatigue life of woven fabric carbon/epoxy laminates under alternating R-ratio loading along non-proportional path in the σ_m-σ_a plane, *International Journal of Fatigue*, 112 (2018) 36-51.

[16] A. A. R. Broer and D. Zarouchas, Adapted anisomorphic model for fatigue life prediction of CFRP laminates under constant amplitude loading, *International Journal of Fatigue*, 126 (2019) 270-283.

[17] C. Kassapoglou, Fatigue life prediction of composite structures under constant amplitude loading, *Journal of Composite Materials*, 41 (22) (2007) 2737-2754.

[18] C. Kassapoglou, Fatigue model for composites based on the cycle-by-cycle probability of failure: implications and applications, *Journal of Composite Materials*, 45 (3) (2011) 261-277.

[19] A. P. Vassilopoulos, B. D. Manshadi and T. Keller, Influence of the constant life diagram formulation on the fatigue life prediction of composite materials, *International Journal of Fatigue*, 32 (4) (2010) 659-669.

[20] A. P. Vassilopoulos, B. D. Manshadi and T. Keller, Piecewise non-linear constant life diagram formulation for FRP composite materials, *International Journal of Fatigue*, 32 (10) (2010) 1731-1738.
[21] J. F. Mandell, D. D. Samborsky, P. Agastra, A. T. Sears and T. J. Wilson, *Analysis of SNL/MSU/DOE Fatigue Database Trends for Wind Turbine Blade Materials*, SAND2010-7052, Sandia National Laboratories.
[22] J. F. Mandell, D. D. Samborsky, D. A. Miller, P. Agastra and A. T. Sears, *Analysis of SNL/MSU/DOE Fatigue Database Trends for Wind Turbine Blade Materials, 2010-2015*, SAND2016-1441, Sandia National Laboratories.
[23] *SNL/MSU/DOE 2019 Composite Material Database*, Version 29.0, https://www.montana.edu/composites/.

Yuanchen Huang is a lecturer at the Department of Mechanical Engineering, University of Shanghai for Science and Technology, Shanghai, China. He received his B.Eng. from Shanghai Jiao Tong University, China and his M.S. and Ph.D. in Mechanical Engineering from Hanyang University, Korea. His research interests include micromechanics, multi-scale modeling of composite materials, and strength and fatigue life prediction of composite structures.

Sung Kyu Ha is a Professor at the Division of Mechanical Engineering, College of Engineering, Hanyang University, Seoul, Korea. He received his B.Eng. from Hanyang University, Korea and his M.S. and Ph.D. in Mechanical Engineering from Stanford University. His research interests include integrated engineering development process for highly competitive composites, innovative additive manufacturing of composites, integrated design optimization of wind turbine blades, design of flywheel energy storage systems, multi-scale fatigue life prediction of composites, and structural health monitoring.